JCTC Journal of Chemical Theory and Computation

Calculation of One-Photon and Two-Photon Absorption Spectra of Porphyrins Using Time-Dependent Density Functional Theory

Paul N. Day,*[,†,‡] Kiet A. Nguyen,[†,§] and Ruth Pachter*[,†]

Materials and Manufacturing Directorate, Air Force Research Laboratory, Wright Patterson Air Force Base, Ohio 45433, General Dynamics Information Technology, Inc., Dayton, Ohio 45431, and UES, Inc., Dayton, Ohio 45432

Received March 6, 2008

Abstract: Time-dependent density functional theory has been used to calculate the one-photon and two-photon absorption spectra of free-base porphyrin, a substituted zinc porphyrin, and a zinc porphyrin dimer, in order to assess the validity of the method to reproduce the large increase in the two-photon absorption (TPA) cross-section for the dimer. Three hybrid functionals with varying amounts of exact exchange were tested, and the calculated one-photon absorption spectra for each of the molecular systems were shown to be in qualitative agreement with the measured spectra. All three functionals predict a large enhancement in the TPA cross-section for the dimer relative to the monomer, in agreement with experimental results. However, because of the sensitivity of the resonance enhancement factor to small differences in the relevant state energies, quantitative prediction of the TPA cross-section by this method is still a challenge.

I. Introduction

Porphyrin systems are important in a variety of biological functions; for example, because of their combination of biocompatibility and nonlinear optical properties, they have been used in photodynamic therapy.[1–4] Photofrin,[5] a porphyrin oligomer, has been approved for the treatment of some forms of cancer. Porphyrins have long been studied also for nonlinear absorption, such as reverse-saturable absorption[6–8] due to excited-state absorption, but were not found useful for two-photon absorption (TPA). However, a remarkable enhancement in the TPA cross-section in porphyrin dimers linked by ethyne or butadiyne has been observed in recent studies.[9–11]

Drobizhev et al.[11] measured the one-photon absorption (OPA) and TPA spectra of a porphyrin monomer, [5,15-bis(3,5-bitert-butylphenyl)-10,20-bis(trihexylsilylethynyl)porphyrinato]zinc, labeled yPy, and several porphyrin dimers, the simplest of which is 5,5′-(ethyne)bis[[10,20-bis(3,5-bitert-butylphenyl)-porphyrinato]zinc], labeled PyP (see Figure 1). The maximum TPA cross-section measured for PyP was about 350 times the maximum TPA cross-section of yPy. In this work, we aim to assess time-dependent density functional theory (TDDFT) for the prediction of OPA and TPA spectra for the porphyrin monomer and dimer, in particular, the enhancement of the TPA cross-section for PyP as compared to yPy.

For comparison, we also discuss the simplest porphyrin, free-base porphin (FBP, see Figure 1), for which numerous excited-state studies have been carried, in part due to the availability of experimental gas-phase UV−vis spectra.[12] In addition, results for the Q band are available that were measured in a supersonic expansion,[13] and they are in good agreement with previous measurements in the gas phase.[12] The theoretical methods that have been used for FBP include complete-active-space with second-order perturbation corrections (CASPT2),[14–16] symmetry-adapted-cluster configuration interaction (SAC-CI),[15,17–20] similarity-transformed equation-of-motion coupled-cluster (STEOM-CC),[21] quantum Monte Carlo (QMC),[22] the semiempirical CNDO-π-SCF-MO-PSDCI method,[23] and TDDFT.[15,24–29] In this paper, the body of spectral data on FBP will be reviewed

* Corresponding authors. E-mail: Paul.Day@wpafb.af.mil (P.N.D.); Ruth.Pachter@wpafb.af.mil (R.P.).

† Air Force Research Laboratory

‡ General Dynamics Information Technology, Inc.

§ UES, Inc.

10.1021/ct800080w CCC: $40.75
Published on Web 06/10/2008

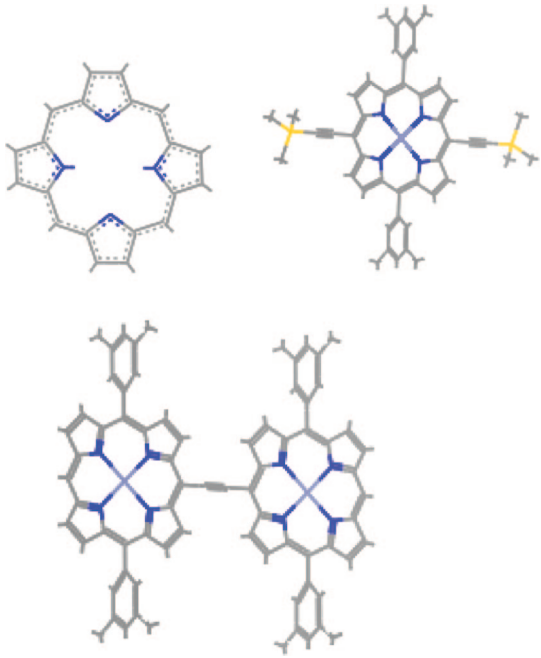

Figure 1. Structure of FBP, yPy, and PyP.

and expanded upon, with the goal of determining the appropriate exchange-correlation (x-c) density functional and basis set to be used to provide reliable spectra for larger porphyrins.

II. Theory

The TPA cross-section is calculated by the expression given previously,[30–33]

$$\delta_{f0}(E_1+E_2)=\frac{8\pi^4}{(ch)^2}E_1E_2g(E_1+E_2)|S_{f0}(u_1,u_2)|^2 \quad (1)$$

where g is a line width function, $|S_{f0}(u_1,u_2)|^2$ is the two-photon probability corresponding to a transition from the ground state (0) to a final state (f),[23,34–41]

$$|S_{f0}(u_1,u_2)|^2=\left|\sum_i^N\left[\frac{(u_1\cdot\mu_{i0})(\mu_{fi}\cdot u_2)}{E_i-E_1+i\Gamma_i}+\frac{(u_2\cdot\mu_{i0})(\mu_{fi}\cdot u_1)}{E_i-E_2+i\Gamma_i}\right]\right|^2 \quad (2)$$

and E_1 and $E_2$are the energies of the two photons with unit polarization vectors u_1 and u_2, respectively. The transition dipole moments are given by μ_{ij}, and the state energies and line widths are given by E_i and Γ_i, respectively. As we noted previously,[32,33] electronic spectra can be obtained from linear response (LR) TDDFT, while TPA cross-sections require the application of quadratic response theory. The two-photon probabilities can be evaluated by the above sum-over-state (SOS) expression, or directly from the single residue of the quadratic response (SRQR)[42–44] in TDDFT. To carry out the SOS, the ground-to-excited-state transition dipole moments needed are obtained from LR TDDFT, while the excited-state to excited-state moments are obtained from the double residue of the quadratic response (DRQR).

The line shape can be represented by a Gaussian function:

$$g^{\mathrm{G}}(E_1+E_2)=\left(\frac{4h^2\ln 2}{\pi E_{\mathrm{FWHM}}^2}\right)^{\frac{1}{2}}\exp\left[\frac{-4\ln 2}{E_{\mathrm{FWHM}}^2}(E_1+E_2-E_f)^2\right] \quad (3)$$

or by a Lorentzian:

$$g^{\mathrm{L}}(E_1+E_2)=\frac{h}{\pi}\frac{E_{\mathrm{FWHM}}/2}{(E_1+E_2-E_f)+(E_{\mathrm{FWHM}}/2)^2} \quad (4)$$

where E_{FWHM} is the full-width at half-maximum for the final state f, and E_f is the energy of state f relative to the ground state. Note that, when a Gaussian function is used, the calculated peak TPA cross-section is 1.48 times larger than for a Lorentzian, for a given line width.

The TPA probability is dependent on the orientation of the molecule relative to the incident photons, so orientationally averaged expressions have been derived for various beam orientations and polarizations.[39] To correspond with experimental results, the expression used here is for photons that are linearly polarized with parallel polarization.

TPA processes can be divided into type I and type II.[32,45,46] In centrosymmetric molecules, the ground state has gerade symmetry, and only states with ungerade symmetry are one-photon-allowed, while only states of gerade symmetry are two-photon-allowed. The TPA in centrosymmetric molecules is of type I, where the state i in eq 2 must be of ungerade symmetry in order to have a nonzero transition dipole moment with the gerade ground state, and the final state f is of gerade symmetry and thus has a nonzero transition dipole moment with state i. The type I TPA cross-section can be estimated by the three-state approximation, which assumes that a single term dominates the sum in eq 2, and in the case where the two photons have the same energy (E_λ), the cross-section is given by

$$\delta_{f0}^{\mathrm{I}}=\frac{32\pi^4 g_{\max}}{15(ch)^2}\frac{E_\lambda^2}{(E_i-E_\lambda)^2}|\mu_{0i}|^2|\mu_{if}|^2(2\cos^2\Theta_{\mu\mu}+1) \quad (5)$$

where $g_{\max}$, the maximum in the line width function, is obtained by setting $E_f = E_1 + E_2 = 2E_\lambda$ in eq 3 or 4, and $\Theta_{\mu\mu}$ is the angle between the two transition dipole moment vectors. While the three-state approximation is often not adequate for quantitative results, it can be useful in analyzing the origin of the TPA intensity.

Type II TPA occurs in noncentrosymmetric molecules where there is a change in the dipole moment between the ground state and the final state. In this case, the sum may be dominated by the terms from these two states, and a two-state approximation to the TPA cross-section may be used:

$$\delta_{f0}^{\mathrm{II}}=\frac{32\pi^4 g_{\max}}{15(ch)^2}|\mu_{0f}|^2|\Delta\mu_{0f}|^2(2\cos^2\Theta_{\mu\Delta\mu}+1) \quad (6)$$

where $\Delta\mu_{0f}=\mu_{ff}-\mu_{00}$, and $\Theta_{\mu\Delta\mu}$ is now the angle between the transition dipole moment and the dipole difference vectors. Although not all of the systems in this study are strictly centrosymmetric, such as the yPy(1p) molecular

system, they have enough symmetry that type I TPA is the dominant process.

III. Computational Methods

The geometry of each molecular system was optimized using the B3LYP functional with the 6-31G** basis set. Geometry optimizations and some LR TDDFT calculations were carried out with Gaussian 03.[47] LR, SRQR, and DRQR TDDFT calculations were carried out with the Dalton program.[48] The DRQR calculations were used to investigate the minimal-states approximations and also to check the TPA cross-sections obtained by the SRQR method, and good convergence of the SOS in the DRQR method was found with less than 20 excited states. All of the calculated TPA cross-sections reported here use the more efficient SRQR method. Gaussian line-width functions were used to compute the TPA cross-sections, with the line widths obtained from the experimental TPA spectra for yPy and PyP.[11] For FBP, no experimental line width is available, so we used a line width of 0.26 eV to be consistent with the previous theoretical study[23] and because it is a reasonable approximation to the TPA line width observed in the experimental studies on FBTPP.[1,49] Generalized gradient approximation (GGA) functionals such as BLYP[50,51] were tested for the TDDFT calculations but were found to be unsatisfactory due to the number of so-called "ghost" states produced near the position of the strong B band. These "ghost" states, which are clearly artifacts of the functional as based on results from both experiments and other levels of theory, have been previously noted with the use of GGA functionals for FBP.[29]

The functionals used for the TDDFT calculations were B3LYP,[50–54] CAMB3LYP,[55–58] and mCAMB3LYP.[33,59] The B3LYP functional is the most widely used "hybrid" functional, where a fraction of exact exchange (0.2 in this case) is combined with a GGA exchange functional to improve its behavior in the asymptotic region. However, to further improve the prediction accuracy of charge-transfer states and Rydberg states, a long-range corrected (LC) functional was recently introduced[60] to increase the fraction of exact exchange in the asymptotic region. This functional was further improved by modification of it into a three-parameter model called the coulomb-attenuated model (CAM).[55] This model used the same Becke exchange[50] and Lee, Yang, and Parr correlation (LYP)[51] used in the B3LYP functional to get the CAMB3LYP[55] functional, which has a fraction of exact exchange that varies from 0.19 (similar to the value in B3LYP) at small separations to 0.65 ($\alpha + \beta$) at large separations (using the default parameter values $\alpha = 0.19$, $\beta = 0.46$, and $\mu = 0.33$). The parameter μ, which scales the separation in the argument to the error function, was kept fixed at 0.33, which had been optimized by Tawada et al.[60] for the first to third row atoms. Other modified forms have been introduced, such as the LC-ωPBE functional of Vydrov and Scuseria,[61] but in a recent assessment,[62] none were found that proved to be superior to CAMB3LYP. However, for many molecules with intramolecular charge transfer, carrying out TDDFT with the standard CAMB3LYP functional (where $\beta = 0.46$) yields excitation spectra in poorer agreement with experimental results than when the B3LYP functional is used, so a modified version of this functional was introduced and tested (mCAMB3LYP)[33,59] with $\beta = \alpha = 0.19$, making it a two-parameter LC model with the maximum fraction of exact exchange equal to 0.38.

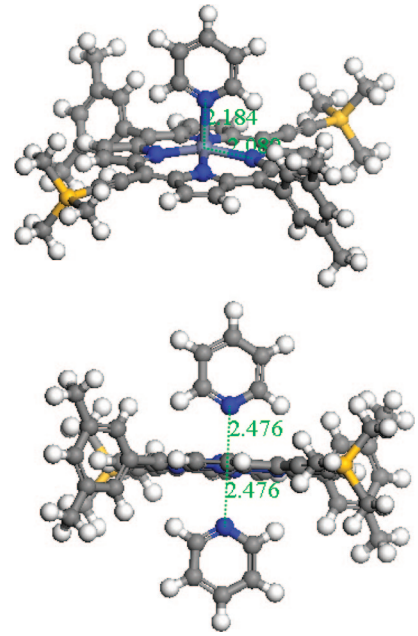

Figure 2. Structure of yPy(1p) and yPy(2p).

Two continuum solvation models were tested, namely, the self-consistent reaction field model with a spherical cavity (SCRF-S) by Mikkelson et al.,[63,64] which has been implemented in Dalton 2.0,[48] and the polarizable continuum model (PCM),[65,66] which was used previously[67] with TDDFT to improve the agreement with measured spectra of substituted porphyrins in chloroform. The PCM was used in both Gaussian 03[47] and in a developmental version of Dalton.[68] The internally stored parameters for the experimental solvent of interest, dichloromethane (aka methylene chloride), were used and are consistent between the two programs. The value used for the static dielectric constant was 8.93, and for the optical-frequency dielectric constant, a value of 2.02 was used. In our reported calculations, model compounds were used with methyl groups substituted for the hexyl and *tert*-butyl groups on yPy and PyP. Note that the solvent in the experimentally measured OPA and TPA spectra for the zinc porphyrin systems was dichloromethane with 1% pyridine,[11] presumably to prevent aggregation by coordinating with the zinc atoms in the porphyrin. In order to simulate the effect of the pyridine, the geometry of yPy was reoptimized with one and two pyridine molecules coordinated to the zinc atom to form the structures yPy(1p) and yPy(2p), respectively (see Figure 2). At the given level of theory (B3LYP/6-31G**), both of these structures are about 15 kcal/mol more stable than the noncoordinated molecules. However, the bond between the pyridine and the Zn atom in yPy(1p) is shorter (2.1 Å) and stronger than the corresponding bonds (2.5 Å) in yPy(2p). Results will be reported for the bare yPy molecule and for yPy(1p), to assess the effects of a coordinating ligand.

If the isolated PyP molecule is held flat, enforcing D_{2h} symmetry, the resulting stationary point has several imaginary frequencies, and thus it is not a minimum, but is 3.1

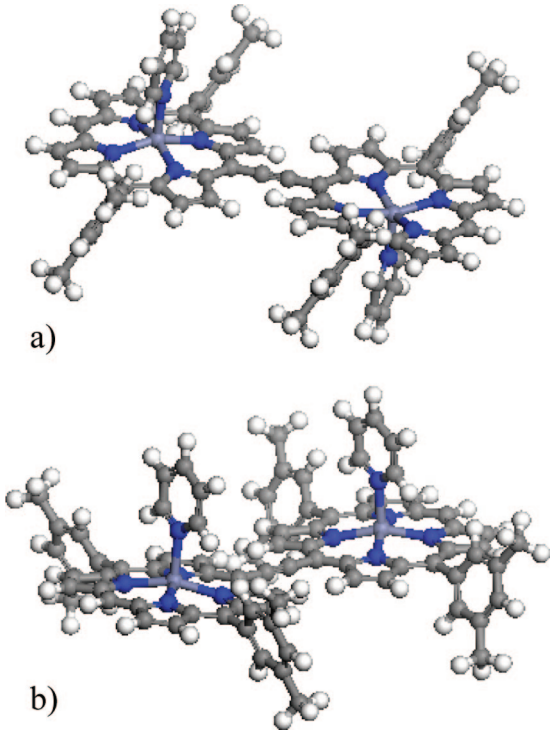

Figure 3. Structure of PyP(2p) with symmetry (a) C_{2h} and (b) C_{2v}.

kcal/mol higher in energy than the minimum energy structure. In the minimum energy structure, the two porphyrin planes are twisted 36° from each other, as was found previously at the AM1[11,69] and B3LYP[70] levels for this molecule. Structures with two pyridine molecules coordinated with PyP, one to each zinc atom, as is shown in Figure 3, have been optimized in C_{2v} symmetry (with the two pyridine molecules on the same side) and in C_{2h} symmetry (with the pyridine molecules on opposite sides). The C_{2h} structure was found to be 1.5 kcal/mol lower in energy than the C_{2v} structure, so it was used in further calculations reported here. A TDDFT calculation was carried out also for the C_{2v} structure using the B3LYP functional, and the OPA spectra are nearly identical to the spectra obtained using the C_{2h} geometry. However, the C_{2h} geometry has several small imaginary frequencies and is still about 0.8 kcal/mol higher in energy than the minimum energy geometry, which has the two porphyrin planes twisted by 31°. Results for both the C_{2h} geometry and the minimum-energy C_1 geometry will be presented here. While the results from the C_1 geometry are expected to be in better agreement with experimental results, the results from the C_{2h} geometry should give the maximum nonlinear absorption to be expected for this molecule, as the planar structure maximizes conjugation and π-orbital delocalization. This may be closer to what would be seen in a solid crystal. Also, the calculations in the higher symmetry aid in identifying and classifying the excited states. Coordinates for all structures are given in the Supporting Information.

The largest calculations carried our here, the quadratic TDDFT on PyP(2p) with no symmetry, took 96 h on 32 processors on an SGI Altix. The linear TDDFT calculations could be carried out at approximately one-fourth the cost of the quadratic TDDFT. Also, calculations on the porphyrin monomer system yPy(1p) required only about 20% of the computational effort of the porphyrin dimer system.

IV. Results and Discussion

A. Free-Base Porphyrin (FBP). *1. OPA.* The calculated excitation energies and oscillator strengths for free-base porphyrin (FBP), also known as porphin, are listed in Table 1 and compared to experimental results and previous calculations. The results for the B3LYP and CAMB3LYP functionals agree with those reported previously[15,26,29] using the 6-31G(d) basis set (although the assignment of the B and N states with B3LYP was reversed by Cai et al.[15]). The results with the 6-311G(d,p) basis show that the basis set effects are small, as was previously shown for this molecule using TDDFT with nonhybrid density functionals.[25,29]

The spectra of porphyrins is typically interpreted through the Gouterman four-orbital model (GFOM).[12,71] In FBP, which has D_{2h} symmetry, the two highest occupied molecular orbitals, the HOMO ($5b_{1u}$) and HOMO-1 ($2a_u$), and the two lowest unoccupied molecular orbitals, LUMO ($4b_{3g}$) and LUMO+1 ($4b_{2g}$) are significantly separated in energy from the other orbitals and play a major role in explaining the spectral features. The HOMO and HOMO-1 are nearly degenerate as are the LUMO and LUMO-1, and transitions between these four orbitals are used to explain the Q and B bands in porphyrin spectra. For FBP, each band consists of "*x*" (excitation parallel to the inner hydrogen−hydrogen axis with B_{3u} symmetry, see Figure 1) and "*y*" (perpendicular to the inner hydrogen−hydrogen axis with B_{2u} symmetry) components. At the lower energy, the transitions interfere destructively, and thus the Q band is very weak, while the B band is strong due to constructive interference.

The vapor-phase excitation energies predicted using the B3LYP functional are in excellent agreement with experimental results for both the Q and B bands, consistent with previous calculations,[15,24,26,29] while in the CAMB3LYP results, the excitation energy of the B band is slightly overestimated, similar to that obtained in the high-level ab initio methods SAC-CI,[15] CASPT2,[15] and STEOM-CC.[21] The measured intensity of the Q band is several orders of magnitude larger than calculated, likely due to vibronic coupling, an effect not included in the calculations. The total oscillator strength calculated for the B band using B3LYP (1.04) is in good agreement with the measured value (1.15), while CAMB3LYP overestimates the oscillator strength by about 70%, and CASPT2,[15] STEOM-CC,[21] and CAS-CI[15] overestimate it by 50%, 65%, and 110%, respectively. The mCAM results are intermediate to B3LYP and CAMB3LYP, overestimating the B-band oscillator strength by about 40%.

In the experiment, the N band is a small shoulder on the B band with an estimated maximum at 3.65 eV, while in the calculations, the N band is a distinct peak of intensity comparable to the B band (depending on the functional used). The N band is still close in energy to the B band, and it appears there could be some mixing of the orbitals involved in these transitions. The major contributions to each of these excited states from each orbital transition for the three

Table 1. Excitation Energies (ΔE in eV) and Oscillator Strengths (f) for Porphin Calculated by TDDFT and Compared to Other Levels of Theory and Experiment

	basis		1^1B_{3u} Q_x	1^1B_{2u} Q_y	2^1B_{3u} B_x	2^1B_{2u} B_y	3^1B_{2u} N_y	3^1B_{3u} N_x
CNDO-CI[23]		ΔE	1.85	2.53	3.23	3.49	3.98	3.83
		f	0.00	0.06	0.32	0.73	0.88	1.30
B3LYP[24]	SVP	ΔE	2.27	2.43	3.32	3.49		
B3LYP[29]	SVP	ΔE	2.24	2.39	3.27	3.45	3.70	3.79
		f	0.00	0.00	0.40	0.61	0.55	0.82
B3LYP[15,26]	6-31G*	ΔE	2.28	2.44	3.34	3.51	3.77	3.87
		f	0.00	0.00	0.42	0.63	0.51	0.78
B3LYP[a]	6-31G*	ΔE	2.28	2.44	3.33	3.51	3.77	3.86
		f	10^{-6}	10^{-5}	0.41	0.63	0.51	0.78
B3LYP[a]	6-311G**	ΔE	2.27	2.42	3.31	3.48	3.74	3.83
		f	10^{-6}	10^{-5}	0.44	0.67	0.48	0.76
B3LYP/PCM[a,b]	6-311G**	ΔE	2.29	2.43	3.23	3.33	3.74	3.73
		f	10^{-4}	10^{-4}	0.94	1.27	0.20	0.61
CAMB3LYP[15]	6-31G*	ΔE	2.19	2.42	3.55	3.69	4.50	4.28
		f	0.00	0.00	0.81	1.16	0.07	0.59
CAMB3LYP[a]	6-31G*	ΔE	2.19	2.42	3.55	3.69	4.50	4.27
		f	10^{-3}	10^{-3}	0.80	1.16	0.07	0.59
CAMB3LYP[a]	6-311G**	ΔE	2.17	2.39	3.52	3.65	4.46	4.24
		f	10^{-3}	10^{-3}	0.83	1.17	0.07	0.57
CAM/PCM[a,b]	6-311G**	ΔE	2.19	2.38	3.37	3.44	4.49	4.19
		f	10^{-3}	10^{-3}	1.30	1.49	0.06	0.43
mCAM[a]	6-31G*	ΔE	2.27	2.45	3.44	3.61	4.05	4.03
		f	10^{-4}	10^{-4}	0.60	1.00	0.19	0.69
mCAM[a]	6-311G**	ΔE	2.25	2.43	3.41	3.57	4.02	4.00
		f	10^{-4}	10^{-4}	0.63	1.02	0.18	0.67
mCAM/PCM[a,b]	6-311G**	ΔE	2.27	2.43	3.29	3.38	4.05	3.92
		f	10^{-7}	10^{-3}	1.13	1.40	0.11	0.50
SAC-CI[15]	6-31G*	ΔE	1.71	2.10	3.46	3.61	4.19	4.09
		f	0.00	0.00	1.00	1.49	0.36	0.89
SAC-CI[15]	6-31G	ΔE	1.80	2.29	3.62	3.77	4.39	4.22
		f	0.00	0.00	1.10	1.64	0.27	0.85
CASPT2[15]	6-31G	ΔE	1.84	2.24	3.56	3.12	3.95	3.72
		f	0.00	0.01	0.98	0.76	0.51	0.03
CASPT2[14]	SV(d)	ΔE	1.63	2.11	3.12	3.08	3.42	3.53
		f	0.00	0.00	0.70	0.91	0.46	0.83
SAC[17]	SV(d)	ΔE	1.77	2.01	3.47	3.73	4.38	4.20
		f	0.00	0.01	0.77	1.62	0.34	1.32
STEOM-CC[21]	DZP	ΔE	1.75	2.40	3.47	3.62	4.35	4.06
		f	0.00	0.01	0.69	1.20	0.42	0.93
QMC[22]		ΔE (eV)		2.46				
		f						
measured[12]		ΔE (eV)	1.98	2.42	3.33		3.65	
		f	0.01	0.06	1.15		0.10	
measured[13]		ΔE (eV)	2.02	2.47				
Measured (in CH_2Cl_2)[12]		ΔE (eV)	2.02	2.39	3.15			

[a] Current work. [b] The PCM solvation model for CH_2Cl_2 was included.

functionals are given in Table 2. The two GFOM transitions are listed first for each state. For all three functionals, the first two excited states have only GFOM transitions as significant contributers, thus clearly defining the Q band.

In a recent study,[15] when the B3LYP functional was used, the third and fourth excited states were assigned to the N band, while the fifth and sixth excited states were assigned to the B band, which is the opposite of the assignments in three earlier B3LYP studies.[24,26,29] The assignments here are consistent with the earlier studies.[24,26,29] When the B3LYP functional is used, a transition from a non-Gouterman orbital (HOMO-2) has the largest contribution to the third excited state, but the two GFOM transitions have comparable contributions, and this is identified as the B_x state. The situation is similar for the fourth excited state, where the two GFOM transitions and a transition from HOMO-2 all have significant and comparable contributions, and this state is identified as B_y. The next two states have smaller contributions from the GFOM transitions, with larger contributions from the previously mentioned transitions from HOMO-2, so these states are labeled N_y and N_x. When the CAMB3LYP functional is used, the contributions from the GFOM transitions for the third and fourth excited states are clearly dominant, leaving no doubt that this is the B band, and there is much less mixing of the GFOM transitions into the N band. The results using the mCAM functional are intermediate relative to the other two functionals, but the GFOM transitions are still the largest contributers to the third and fourth excited states, verifying their assignment to the B band, and there is less mixing of the GFOM into the N-band states than when B3LYP was used. The effect of an applied external field on the calculated states was also tested, in a manner similar to that carried out previously,[15] and while the results showed the B3LYP states to be affected more by

Table 2. Weight Percent Contribution of Each Orbital Transition for Each Excited State of Porphin[a]

		CASPT2[14]	B3LYP[b]	CAMB3LYP[b]	mCAM[b]
1^1B_{3u}	**Q_x**	**1.630**	**2.281**	**2.186**	**2.268**
H → L + 1	$5b_{1u} \rightarrow 4b_{2g}$	0.370	0.293	0.270	0.283
H − 1 → L	$2a_u \rightarrow 4b_{3g}$	0.340	0.204	0.231	0.214
1^1B_{2u}	**Q_y**	**2.110**	**2.442**	**2.417**	**2.454**
H → L	$5b_{1u} \rightarrow 4b_{3g}$	0.410	0.272	0.252	0.264
H − 1 → L + 1	$2a_u \rightarrow 4b_{2g}$	0.390	0.225	0.246	0.233
2^1B_{3u}	**B_x**	**3.120**	**3.335**	**3.553**	**3.436**
H → L + 1	$5b_{1u} \rightarrow 4b_{2g}$	0.130	0.111	0.180	0.144
H − 1 → L	$2a_u \rightarrow 4b_{3g}$	0.280	0.191	0.238	0.221
H − 2 → L + 1	$4b_{1u} \rightarrow 4b_{2g}$	0.270	0.294	0.084	0.136
2^1B_{2u}	**B_y**	**3.080**	**3.511**	**3.693**	**3.607**
H → L	$5b_{1u} \rightarrow 4b_{3g}$	0.210	0.177	0.253	0.232
H − 1 → L + 1	$2a_u \rightarrow 4b_{2g}$	0.300	0.195	0.256	0.253
H − 2 → L	$4b_{1u} \rightarrow 4b_{3g}$	0.170	0.136	0.007	0.028
3^1B_{2u}	**N_y**	**3.420**	**3.770**	**4.495**	**4.045**
H → L	$5b_{1u} \rightarrow 4b_{3g}$		0.053		0.008
H − 1 → L + 1	$2a_u \rightarrow 4b_{2g}$	0.070	0.083	0.005	0.018
H − 2 → L	$4b_{1u} \rightarrow 4b_{3g}$	0.320	0.357	0.452	0.459
H − 7 → L	$3b_{1u} \rightarrow 4b_{3g}$	0.150	0.012	0.033	0.013
3^1B_{3u}	**N_x**	**3.530**	**3.865**	**4.274**	**4.031**
H → L + 1	$5b_{1u} \rightarrow 4b_{2g}$	0.220	0.101	0.062	0.081
H − 1 → L	$2a_u \rightarrow 4b_{3g}$	0.090	0.108	0.041	0.071
H − 2 → L + 1	$4b_{1u} \rightarrow 4b_{2g}$	0.290	0.294	0.377	0.347

[a] Excited state energies (in eV) are given in bold. [b] Current work.

the applied field than the CAMB3LYP states, the results did not motivate a change in the assignment of the calculated states. Note, however, that, while the B3LYP functional gives the most accurate excitation energy and intensity for the B band, it also yields a more intense N band, which is qualitatively incorrect. The CAMB3LYP functional overestimates the excitation energy and intensity of the B band more than the other two functionals, and thus the mCAM functional could be a compromise for the prediction of spectra in porphyrins.

The effect of a solvent on the spectra was investigated using the PCM with each of the three density functionals, and comparing the results to the spectra measured for FBP in dichloromethane.[12] The PCM successfully predicts the very small blue shift of the Q_x state, the very small red-shift of the Q_y state, and the red-shift of nearly 0.2 eV for the B band. When the PCM is included in the calculation, the strength of the B band is significantly larger than that of the N band, which is in better qualitative agreement with experimental results.

2. TPA. The maximum TPA cross-sections for FBP calculated using the B3LYP, CAMB3LYP, and mCAMB3LYP functionals are given in Table 3, along with the calculated results from a previous study[23] using CNDO-π-SCF-MO-PSDCI and SOS and the measured peak TPA cross-sections for a similar molecule, free-base meso-tetraphenylporphin (FBTPP).[1,49] The CNDO study[23] used an alternative definition of the TPA cross-section, which gives values twice as large as with our convention, as we have mentioned previously;[32,33] thus, their reported values have been corrected for this factor for direct comparison to our results. The calculated TPA cross-section using B3LYP of 17.3 GM for the A_g state at 4.27 eV is similar in magnitude to the peak TPA cross-section measured for FBTPP.[1,49] However, when the CAMB3LYP and mCAMB3LYP functionals are used, resonance effects dominate the TPA cross-section.

Table 3. Calculated TPA Resonance Transition Energies (ΔE, in eV) and the Corresponding TPA Cross-Sections (σ, in GM) for FBP, Using the 6-31G* Basis, with Comparison to Measured TPA Peak Cross-Sections for a Similar Molecule, FBTPP[a]

		$1A_g$	$2A_g$	$3A_g$	$4A_g$	$5A_g$
measured[1,49] (FBTPP)	ΔE	3.25				
	σ	25				
CNDO-CI[23] reported	ΔE	3.26	3.46	3.82		
	σ	13.76	1.05	585.71		
corrected	σ	6.88	0.53	292.85		
B3LYP	ΔE	3.61	4.27	4.44	4.85	5.19
	σ	0.28	17.28	1.53	0.45	13.94
CAMB3LYP	ΔE	4.38	4.87	5.28	5.42	5.92
	σ	157451	137.67	4.13	3.00	3.57
mCAMB3LYP	ΔE	3.93	4.54	4.79	5.08	5.47
	σ	0.55	136.52	3.82	0.08	7.07

		$1B_{1g}$	$2B_{1g}$	$3B_{1g}$	$4B_{1g}$	$5B_{1g}$
CNDO-CI[23] reported	ΔE	3.13	3.49	3.84	3.91	
	σ	1.58	0.61	23.27	50.33	
corrected	σ	0.79	0.31	11.63	25.16	
B3LYP	ΔE	3.42	4.05	4.25	4.68	5.23
	σ	0.00	11.44	0.15	0.03	9.82
CAMB3LYP	ΔE	3.88	4.77	4.87	5.29	6.09
	σ	0.02	2.82	222.52	2.60	9.83
mCAMB3LYP	ΔE	3.61	4.38	4.49	4.93	5.62
	σ	0.01	13.57	0.66	13.41	32.55

[a] A Gaussian lineshape was used with FWHM = 0.26 eV. The CNDO-CI[23] cross-sections have been corrected for consistency with our definition (see text).

When CAMB3LYP is used, the computed A_g TPA state at 4.38 eV is nearly exactly resonant with the computed Q_x state at 2.19 eV. Similarly for mCAMB3LYP, a TPA state with A_g symmetry is computed at 4.54 eV, which is nearly perfectly resonant with the computed Q_x state at 2.27 eV. The calculation of such large, unphysical TPA cross-sections for these states illustrates the importance of accurately

Table 4. Calculated Excitation Energies (ΔE in eV) and Oscillator Strengths (f) for yPy Compared to Experiments[a]

solvent[b]		basis		Q_x	Q_y	B_y	B_x	
none	CV-INDO-CI[70]		ΔE	2.07		3.15	3.19	
			f	0.03		1.73	2.09	
none	B3LYP	6-31G**	ΔE	2.17	2.19	3.07	3.16	
			f	0.19	0.00	1.22	1.47	
1p	B3LYP	6-31G**	ΔE	2.09	2.14	2.99	3.11	
			f	0.21	0.00	0.99	1.14	
1p + PCM	B3LYP	6-31G**	ΔE	2.05	2.14	2.87	2.99	
			f	0.31	0.00	1.31	1.41	
none	CAMB3LYP	6-31G**	ΔE	2.18	2.20	3.33	3.34	
			f	0.14	0.01	1.37	1.77	
1p	CAMB3LYP	6-31G**	ΔE	2.07	2.14	3.19	3.26	
			f	0.17	0.00	1.24	1.47	
1p + PCM	CAMB3LYP	6-31G**	ΔE	2.04	2.13	3.06	3.13	
			f	0.26	0.00	1.52	1.69	
none	mCAMB3LYP	6-31G**	ΔE	2.21	2.23	3.20	3.25	
			f	0.17	0.00	1.24	1.64	
1p	mCAMB3LYP	6-31G**	ΔE	2.10	2.16	3.06	3.19	3.13
			f	0.20	0.00	0.85	1.19	0.45
1p + PCM	mCAMB3LYP	6-31G**	ΔE	2.07	2.16	2.95	3.05	
			f	0.30	0.00	1.41	1.55	
CH_2Cl_2	measured[11]		ΔE	1.92	2.07	2.73	2.80	
			f	0.15	0.00	0.66	0.94	

[a] The isolated yPy molecule has C_{2h} symmetry, and all the excited states reported here have B_u symmetry. When a pyridine molecule is coordinated to yPy, the symmetry is reduced to C_2 and the symmetry of the excited states is B. [b] 1p denotes that one pyridine molecule is coordinated with the Zn atom, as shown in Figure 2. PCM denotes the polarizable continuum model with the parameters for CH_2Cl_2 as the solvent.

obtaining the state energies. Further improvements are needed in the (x-c) functional to be applied for the calculation of TPA cross-sections in porphyrins, as we also demonstrate for yPy and PyP.

B. yPy. *1. OPA.* The addition of the ethynyl groups to the basic zinc porphyrin reduces the symmetry from D_{4h} to D_{2h}, red-shifts both the Q and B bands, and increases the Q-band intensity. While the Q band is still weak compared to the B band, the quasidegeneracy of the Gouterman four orbitals is substantially perturbed by this additional conjugation to remove the near-perfect cancelation of the transition dipoles in the Q band. The role the intensity of the Q band plays in the strength of the TPA can be seen in examining the three-state approximation (eq 5); one of the Q-band states is the primary intermediate state for the lowest TPA bands. Table 4 lists the calculated excitation energies and oscillator strengths for the Q and B states in comparison to experimental results. As was noted by Zhu et al.,[70] the x and y labels in the experimental spectra[11] of yPy were reversed, as the Q_x line is the lower-energy and more intense of the Q states, where the molecule has been aligned such that the x axis is the long molecular axis. The isolated yPy molecule has C_{2h} symmetry, and all of the reported OPA states are of B_u symmetry, while in yPy(1p), the symmetry is reduced to C_2 and the OPA states have B symmetry. As with porphin, the computed excitation energies and intensities are larger than the experimental ones.

The inclusion of a single pyridine molecule coordinated to the zinc atom in yPy produces a significant red-shift. The SCRF-S model[63] in Dalton 2.0 has little effect on the calculated excitation energies, but the PCM model produces a significant red-shift, improving the agreement with experimental results. Note that the inclusion of either of the continuum solvation models increases the calculated intensity. Without including PCM, the calculated B band using the CAMB3LYP functional for yPy(1p) is blue-shifted nearly 0.5 eV from experimental results, compared to about 0.3 eV using the B3LYP functional, with the mCAM result about midway between the two. Previously reported excitation energies calculated using CV-INDO-MRDCI[70] for the isolated yPy are quite close to our results using CAMB3LYP on yPy(1p), also overestimating the B-band energies by about 0.5 eV. The PCM reduces our error to about 0.3 eV for CAMB3LYP and less than 0.2 eV for B3LYP. The calculated Q-band excitation energy is closer to experimental results and less dependent on the functional, as all three functionals predict this excitation energy to be nearly 0.2 eV higher than measured with good agreement with the experimental intensity. When the PCM is included, the error in this energy is reduced to about 0.1 eV, but the predicted intensity is increased to nearly double that found experimentally. In the recently reported CV-INDO-CI calculations, the intensity of the Q band was severely underestimated,[70] while the intensity of the B band was substantially overestimated.

2. TPA. The calculated transition energies for the TPA states and the corresponding resonant TPA cross-sections for yPy and yPy(1p) are listed in Table 5, and the calculated TPA cross-sections for yPy(1p) fitted to Gaussian line shapes are plotted in comparison to experimental results in Figure 4. The isolated yPy molecule has C_{2h} symmetry, and the listed TPA states have A_g symmetry, while yPy(1p) has C_2 symmetry and the TPA states have A symmetry. While the B_g states in C_{2h} symmetry and the B states in C_2 symmetry are not strictly TPA-forbidden, the calculated TPA cross-sections for these states are much smaller than those reported in Table 5.

The recently reported TPA cross-sections calculated using CV-INDO-MRDCI[70] used a Lorentzian line-shape function with a FWHM of 0.2 eV, while we used a Gaussian line-shape function with a FWHM of 0.45 to correspond with experimental results. In order to directly compare the calculated[70] TPA cross-sections with ours, the values have been converted to our line shape by multiplying by the factor $1.48 \times 0.2/0.45$. Both the reported and corrected values are reported in Table 5, while Figure 4 shows only the corrected values. After correction, the first TPA peak at 3.04[70] is in good agreement with experimental results, which is surprising considering the underestimation of the Q-band intensity by this method and its importance in the three-state approximation of the TPA cross-section. A much larger TPA cross-section at 3.78 eV was also reported.

While the reported measured maximum TPA cross-section is about 20 GM at a transition energy of about 2.9 eV (corresponding to degenerate photons at 1.45 eV), the QRSR-TDDFT results predict a larger cross-section at a higher transition energy. Each of the three functionals predicts a peak between 3.8 and 3.9 eV with a cross-section between 100 and 200 GM, as well as a much larger peak in the 4.0−4.5 eV range. The calculated TPA states between 4.09 and 4.31 eV have very large cross-sections due to resonance enhancement from the Q_x state located at about 2.1 eV.

Table 5. Calculated TPA Resonance Transition Energies (ΔE, in eV) and the Corresponding TPA Cross-Sections (σ, in GM) for yPy[a]

solvent[b]								
none	CV-INDO-MRDCI[70]	ΔE	3.04	3.78				
	reported	σ	46	406				
	corrected (see text)	σ	30	266				
none	B3LYP/6-31G**	ΔE	3.34	3.43	3.47	3.62	3.68	
		σ	28.3	0.02	27.5	0.23	107.8	
SCRF	B3LYP/6-31G**	ΔE	3.34	3.43	3.45	3.62	3.68	
		σ	44.4	0.04	35.1	0.34	167.8	
1p	B3LYP/6-31G**	ΔE	3.28	3.32	3.38	3.50	3.60	3.61
		σ	0.26	14.1	4.7	66.0	1.4	4.1
		ΔE	3.61	3.70	3.78	3.82	3.89	3.90
		σ	0.71	50.3	7.6	3.5	15.7	34.9
		ΔE	3.96	3.98	4.14	4.16	4.23	4.31
		σ	1.5	58.73	4.2×10^5	2.7×10^6	1.7×10^4	1082
1p	mCAM/6-31G**	ΔE	3.55	3.61	3.70	3.82	3.92	3.98
		σ	1.8	4.5	0.05	101	8.4	4.6
		ΔE	4.02	4.09	4.11	4.17	4.22	4.24
		σ	2.0	5360	8330	1.3×10^5	1.2×10^9	3.2×10^6
1p	CAMB3LYP/6-31G**	ΔE	3.83	3.90	4.28	4.29	4.31	
		σ	76.6	74.6	5.9×10^7	1.0×10^5	5.4×10^4	
CH_2Cl_2	measured[11]	ΔE	2.93					
		σ	23.7					

[a] The isolated yPy molecules have C_{2h} symmetry, and the symmetry of the listed TPA states is A_g. When the yPy is coordinated with a pyridine molecule, the symmetry of the system is reduced to C_2, and that of the TPA states is reduced to A symmetry. We used a Gaussian lineshape with FWHM = 0.45 eV, except for the states above 4.0 eV, where we used FWHM = 0.03 eV to minimize resonance effects on the rest of the spectrum. [b] See footnote to Table 4.

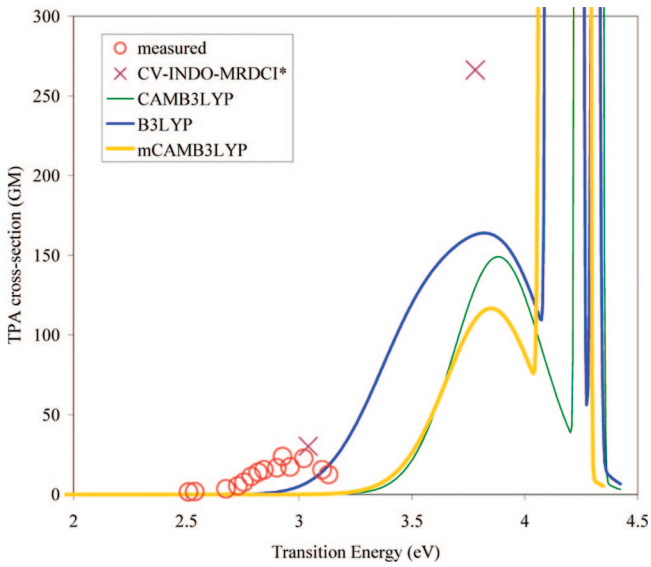

Figure 4. TPA for yPy. The TDDFT calculations have a single pyridine molecule coordinated to the zinc atom. The basis set is 6-31G**, and FWHM = 0.45 eV, except for states above 4.0 eV, where FWHM = 0.03 was used to prevent these states from obscuring the spectra from the lower energy states. The CV-INDO-CI[70] results have been corrected to our line shape function as described in the text.

Experimental TPA is not reported for this range, as OPA will dominate in this energy range. While the experimental FWHM of 0.45 eV has been used for the lower-energy TPA states, a FWHM of 0.03 eV was used for the states between 4.09 and 4.31 eV to prevent them from completely obscuring the lower-energy TPA states. As can be seen in Figure 4, the use of B3LYP results in the highest peak cross-section (164 GM) between 3 and 4 eV, and also the broadest peak. This is due to its being the sum of four major TPA states at 3.50 eV (66 GM), 3.70 eV (50 GM), 3.90 eV (35 GM), and 3.98 eV (59 GM), as well as several minor TPA states. By contrast, the mCAMB3LYP peak of 117 GM is primarily from one TPA state at 3.82 eV (101 GM), and the CAMB3LYP peak of 149 GM is from just two TPA states at 3.83 eV (77 GM) and 3.90 eV (75 GM). This illustrates a major difference in the results from the three functionals: B3LYP yields 14 TPA states below 4.05 eV, mCAMB3LYP yields seven TPA states in this range, and CAMB3LYP gives just two.

The calculated peak TPA cross-section is 5−7 times larger than the measured one and is blue-shifted about 0.8 eV. This overprediction of the TPA cross-section can be attributed to the overprediction of the energy of the two-photon state, thus resulting in a large resonance enhancement factor in eq 5. With some rearrangement, the resonance enhancement factor can be written as

$$\eta = \left(\frac{E_i}{E_f} - 0.5\right)^{-2} \tag{7}$$

where E_i is the energy of the Q_x state, and E_f is the energy of the TPA state. This factor calculated from experimental energies is only 42, but for the four major TPA states calculated using B3LYP, it is 109, 249, 842, and 1659, while for the major TPA state calculated using mCAMB3LYP, it is 396. The CAMB3LYP results illustrate how sensitive to the state energies the calculated TPA cross-section can be due to this resonance enhancement factor, as its value is 576 for the TPA state at 3.83 eV, but for the nearby TPA state at 3.90 eV, it is 1020.

While using the SCRF-S solvation model does not significantly change the calculated state energies, the more accurate PCM can be used to give more accurate state energies. All three functionals, including the PCM, cause a

Table 6. OPA Spectra for PyP Calculated with TDDFT and the 6-31G Basis Set[a]

solvent	functional/sym.		Q_x	Q_x'	B_x	B_x'	N_x	N_x'	M_x	M_x'
none	CV-INDO-CI[70]	ΔE	2.03		2.81	3.60				
		f	0.18		3.24	0.76				
none	B3LYP/D_{2h}	ΔE	1.93		2.80	3.31	2.89		3.47	
		f	0.93		1.01	0.64	0.00		0.14	
2p	B3LYP/C_{2h}	ΔE	1.77	2.46	2.73	3.14	2.86	3.18	3.22	3.36
		f	0.94	0.00	0.84	0.39	0.00	0.07	0.13	0.02
2p	B3LYP/C_1	ΔE	1.84	2.52	2.66	3.12	2.86	3.17	3.19	3.43
		f	0.82	0.00	0.46	0.63	0.00	0.00	0.49	0.00
2p + PCM	B3LYP/C_{2h}	ΔE	1.69	3.05	2.70	3.12	2.89		3.14	3.37
		f	1.20	0.00	0.94	0.49	0.00		0.30	0.01
2p	CAMB3LYP/C_{2h}	ΔE	1.87	3.50	3.00	3.80	4.03	3.70	4.04	4.23
		f	0.71	0.00	1.92	0.31	0.01	0.00	0.03	0.06
2p	CAMB3LYP/C_1	ΔE	1.95		3.01	3.68	3.72			
		f	0.59		1.83	0.24	0.25			
2p + PCM	CAMB3LYP/C_{2h}	ΔE	1.81	3.67	2.94	3.71	4.06	4.04	4.08	
		f	0.94	0.01	2.17	0.28	0.00	0.01	0.01	
2p	mCAMB3LYP/C_{2h}	ΔE	1.83	2.88	2.86	3.46	3.32	3.39	3.70	3.74
		f	0.87	0.02	1.31	0.47	0.00	0.01	0.12	0.00
2p	mCAMB3LYP/C_1	ΔE	1.91		2.83	3.36	3.33	3.39	3.41	
		f	0.75		1.02	0.50	0.01	0.32	0.20	
2p + PCM	mCAMB3LYP/C_{2h}	ΔE	1.76	3.47	2.81	3.40	3.35	3.35	3.68	
		f	1.13	0.03	1.50	0.50	0.02	0.02	0.04	
CH_2Cl_2	experiment	ΔE	1.74	2.16	2.57	2.78				
		f	0.32	0.08	0.76	0.39				

solvent	functional/sym.		Q_y	Q_y'	B_y	B_y'	B_y''	N_y	N_y'	M_y
none	B3LYP/D_{2h}	ΔE	2.15	2.88	2.60	3.42	3.45			
		f	0.01	0.00	0.22	0.08	1.85			
2p	B3LYP/C_{2h}	ΔE	2.01	2.79	2.51	2.95	3.32	3.40	3.01	3.11
		f	0.06	0.17	0.13	0.00	1.60	0.13	0.00	0.04
2p	B3LYP/C_1	ΔE	2.06	2.76	2.51	2.98	3.31		2.52	3.11
		f	0.06	0.16	0.05	0.00	1.58		0.01	0.06
2p + PCM	B3LYP/C_{2h}	ΔE	2.02	2.77	2.49	2.89	3.21	3.40		3.45
		f	0.09	0.29	0.27	0.00	2.11	0.02		0.00
2p	CAMB3LYP/C_{2h}	ΔE	2.16	3.62	3.15	3.55	3.86	4.00	4.10	4.15
		f	0.05	0.47	1.38	0.00	0.70	0.06	0.00	0.02
2p	CAMB3LYP/C_1	ΔE	2.19	3.61	3.21	3.56	3.84	3.59		
		f	0.04	0.33	1.38	0.00	0.52	0.16		
2p + PCM	CAMB3LYP/C_{2h}	ΔE	2.16	3.61	3.04	3.49	3.83	4.15		4.01
		f	0.06	0.50	2.08	0.00	0.60	0.15		0.03
2p	mCAMB3LYP/C_{2h}	ΔE	2.12	3.12	2.80	3.21	3.47	3.68	3.44	3.54
		f	0.06	0.30	0.41	0.00	0.95	0.10	0.01	0.61
2p	mCAMB3LYP/C_1	ΔE	2.16	3.10	2.83	3.23			2.93	
		f	0.05	0.36	0.26	0.00			0.00	
2p + PCM	mCAMB3LYP/C_{2h}	ΔE	2.12	3.10	2.76	3.15	3.41	3.68	3.77	
		f	0.09	0.46	0.81	0.00	1.61	0.04	0.05	
CH_2Cl_2	experiment	ΔE	2.01	2.24	2.64	2.83	3.01			
		f	0.03	0.11	0.38	0.19	1.16			

[a] The excitation energies (ΔE) are in eV. For the cases where the solvent includes two pyridine molecules (denoted "2p"), they are coordinated on opposite sides of the molecule, as shown in Figure 3a.

red-shift of about 0.12 eV for the B band and a red-shift of about 0.04 eV for Q_x. However, the energy shift is much smaller for the TPA states; when the CAMB3LYP is used, each of the first five TPA states is red-shifted by 0.02 eV, while with B3LYP and mCAMB3LYP, we observe similarly small shifts, some in each direction. We conclude that both continuum solvation models predict a significantly larger peak TPA cross-section at about the same transition energy.

C. PyP. *1. OPA.* The calculated and experimental excitation energies and corresponding oscillator strengths for PyP are reported in Table 6. Extinction coefficients are plotted in Figure 5 for the B3LYP functional. Drobizhev et al.[11] reported four excited electronic states with "*x*" polarization (corresponding to the B_u states in the C_{2h} system PyP(2p)) and five excited electronic states with "*y*" polarization (corresponding to the A_u states). The reported combined oscillator strengths[11] of 0.35 for the Q band and 2.91 for the B band were resolved by Gaussian fits into the oscillator strengths reported in Table 6. An oscillator strength of 0.11 for the $Q_x(0-1)$ state at 1.83 eV was combined with an oscillator strength of 0.21 for the $Q_x(0-0)$ state at 1.74 eV.

The B3LYP results with the two different basis sets, 6-31G and 6-31G**, show a small basis set effect, with no change in the position of the Q band and just a small red-shift of the most intense line in the B band with the addition of the polarization functions. There is also a small decrease in the intensity of the Q band and a small increase in the intensity of the B band.

As with yPy, the calculated spectra tend to be blue-shifted and more intense than the measured data. However, the

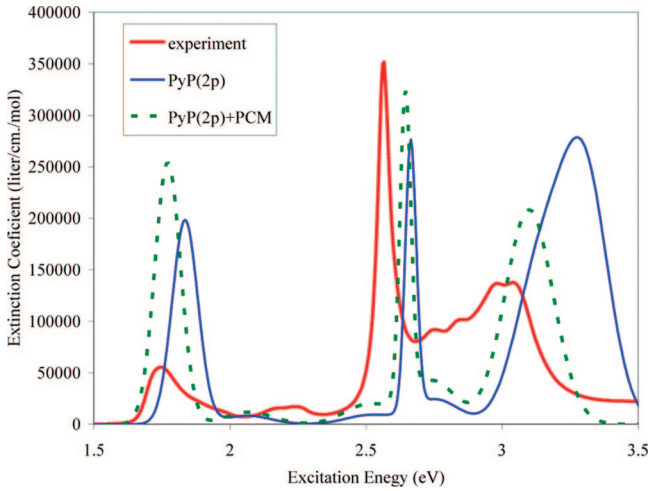

Figure 5. Calculated OPA of PyP(2p) with the B3LYP functional and 6-31G basis set in C_1 symmetry both with and without the PCM solvation model, with comparison to experimental results.

excitation energy calculated for the Q_x state of PyP(2p) with the B3LYP functional using C_{2h} symmetry (either with or without PCM) is in excellent agreement with experimental results, although the calculated oscillator strength (0.9 in the gas phase, 1.1 with PCM) is about 3 times the experimental value (0.32). Allowing the system to relax to the C_1 minimum-energy geometry causes a small blue-shift of 0.1 eV and a small decrease in the oscillator strength to 0.8. Since the amount of charge transfer involved in the Q band is small, the effect of the twisting out of plane of the two porphyrin units and consequent loss in conjugation is also small. Using CAMB3LYP blue-shifts the Q band by about 0.1 eV and reduces the oscillator strength by about 25%. The mCAMB3LYP results fall in between those obtained with B3LYP and CAMB3LYP, with all three functionals in good agreement with the measured Q-band excitation energy while overestimating the oscillator strength. In the previously reported CV-INDO-CI results,[70] the Q_x band position was overestimated by 0.3 eV and the oscillator strength was underestimated by 50%.

The B_x line calculated using B3LYP is in good agreement with experimental results, while the CAMB3LYP functional overestimates the excitation energy and oscillator strength for this transition. Relaxing the symmetry constraint to C_1 substantially decreases the oscillator strength for this line when B3LYP is used, and this intensity appears to be transferred to the B_x' state. Relaxing the symmetry constraint has little effect when the functional is CAMB3LYP; the B3LYP functional predicts more charge transfer in the B-band states than does the CAMB3LYP functional, and thus the loss of conjugation in the C_1 structure has a bigger effect on the B3LYP results. The increased long-range exact exchange in the CAMB3LYP functional decreases charge transfer between the porphyrin units; however, the B3LYP results are in better agreement with the experimental absorption spectra. The results from mCAMB3LYP are again intermediate relative to the other two functionals. In the recent CV-INDO-CI study,[70] the excitation energies calculated for the B_x and B_x' states are higher than experimental results by 0.2 and 0.8 eV, respectively, and the oscillator strengths are overestimated by factors of 4 and 2.

The assignment of the "*y*" polarization states in the B band may seem surprising since the most intense state calculated using B3LYP/PCM (at 3.15 eV) and the most intense state calculated using CAMB3LYP/PCM (at 2.99 eV) are assigned to different states. However, each of the calculated states assigned to the B_y'' line is dominated by the transition from the highest-occupied B_g orbital to the lowest unoccupied B_u orbital. By comparing the results obtained with the mCAMB3LYP functional, we can see how the introduction of the additional asymptotic exchange in the CAM functional induces a transfer of intensity from the B_y'' state to the B_y state. While the states calculated using different functionals can be matched using the calculated molecular orbital transitions, the assignment of the calculated states to experiments is carried out using just the symmetry group, the transition energy, and the oscillator strength. While there are significant differences between the B3LYP and CAMB3LYP for some states, the assignments in Table 6 seem to be the most likely solution.

2. TPA. The TPA resonant cross-sections for PyP are given in Table 7, and fitted TPA cross-sections have been plotted in Figure 6. The CV-INDO-CI results[70] have again been corrected for the different line-shape functions used in that study and ours, this time by multiplying by $1.48 \times 0.20/0.22$. Calculated results are given for both the bare PyP (in D_{2h} symmetry) and the solvated PyP(2p) (in both C_{2h} and C_1 symmetries) using the B3LYP, CAMB3LYP, and mCAMB3LYP functionals. Experimentally, a strong TPA peak is observed reaching 8500 GM near a transition energy of 3.0 eV. The CV-INDO-CI study[70] reported a peak near this energy, but with only about one-fourth the intensity. They also predicted a peak with an intensity similar to that found experimentally, but with a transition energy of 3.7 eV. Using B3LYP for the bare PyP, two smaller TPA peaks are calculated, one about 0.5 eV lower in energy than experimental results and the other 0.5 eV higher than experimental results. Including the two pyridines in the calculation induces a red-shift in the lower TPA peak, and while the position of the second peak does not change, the red-shift in the Q-band state (Table 6) brings it into resonance with this state, thus causing an unphysically large result for this TPA cross-section. As can be seen in Figure 6, there is little difference in the peak at 2.25 eV when the C_1 geometry is used, and the 20 TPA states calculated in C_1 geometry extend to only 3.11 eV, thus missing the large resonance near 3.49 eV. When CAMB3LYP is used to model the bare molecule, the first TPA peak is blue-shifted relative to experimental results, but when the two pyridine molecules are included, excellent agreement with experimental results is obtained. A peak TPA cross-section of about 15 000 GM is predicted near a transition energy of 3.06 eV for the C_{2h} geometry, but the experimental results did not report TPA above 3.0 eV, and the TPA cross-section appears to still be increasing at that energy. When the C_1 geometry is used, there is little change in the transition energy, but the peak TPA cross-section is reduced to about 9000 GM, which also appears to agree well with the available experimental data. Much of this reduction

Table 7. TPA Resonances of PyP with Cross-Sections Greater than 100 GM[a]

solvent									
none		CV-INDO-CI[70]	ΔE	2.96	3.70				
		reported	σ	1755	8022				
		corrected, see text	σ	2354	10762				
none	D_{2h}	B3LYP	ΔE	2.39	2.44	3.51			
			σ	604	1869	561			
SCRF	D_{2h}	B3LYP	ΔE	2.39	2.44	3.49			
			σ	1082	3333	1235			
none	D_{2h}	CAMB3LYP	ΔE	3.25	3.77	3.71	4.05	4.07	4.13
			σ	11234	270	373	41505	1.1E+06	4.3E+05
2p	C_{2h}	B3LYP	ΔE	2.25	2.29	3.36	3.49		
			σ	1904	431	168	1.5E+06		
2p	C_{2h}	CAMB3LYP	ΔE	3.06	3.48	3.57	3.60	3.71	
			σ	15052	174	1693	506	1.0E+06	
					4.00	4.03	4.06	4.33	
					143	102	270	18135	
2p	C_{2h}	mCAMB3LYP	ΔE	2.58	3.46	3.75			
			σ	4330	156	52267			
2p	C_1	B3LYP	ΔE	2.25	2.28				
			σ	1935	289				
2p	C_1	CAMB3LYP	ΔE	3.08	3.59	3.59			
			σ	9087	257	142			
2p	C_1	mCAMB3LYP	ΔE	2.59					
			σ	3565					
CH_2Cl_2	experiment		ΔE	3.02					
			σ	8510					

[a] A Gaussian lineshape was used with FWHM = 0.22 eV, and the 6-31G basis set was used. The second column lists the symmetry used in the calculation.

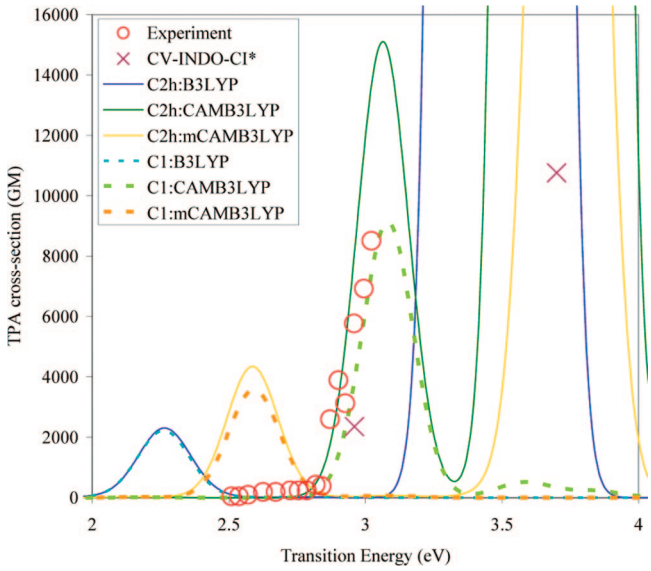

Figure 6. TPA of PyP(2p) calculated using the 6-31G basis and FWHM = 0.22 eV. The experimental data do not extend to transition energies above 3.02 eV. Also, the C_1 calculations do not include enough excited states to reach the highly resonant region of the spectrum. The CV-INDO-CI[70] TPA cross-sections have been corrected to be consistent with our lineshape function (see text).

in the calculated cross-section can be attributed to the decrease in the resonance enhancement factor η (eq 6) of 33%, due to the 0.1 eV blue-shift of the Q_x state (see Table 6). A similar blue-shift in Q_x in the calculation using B3LYP decreases η by 18%, but other factors must compensate for this (perhaps beyond the three-state approximation), since there is no decrease in the calculated TPA cross-section. As the OPA calculated with CAMB3LYP is not in such good agreement with experimental results, the excellent agreement with experimental results of the TPA spectra calculated with CAMB3LYP is still under investigation.

While the B3LYP and mCAMB3LYP functionals underestimate the peak TPA cross-section by factors of 4 and 2, respectively, the main source of the discrepancy appears to be the resonance enhancement factor, as it was in the overestimation of the TPA cross-section of yPy. Most of the enhancement in the TPA cross-section in changing from the monomer to the dimer is in the increase in the magnitudes of the most relevant transition dipole moments. The three-state approximation, eq 5, can be used to understand the source of this enhancement by analyzing the term in the sum with the major contribution to the cross-section. The excited-state transition dipole moment, μ_{if}, can be obtained from a QRDR calculation, while the transition dipole moments from the ground state, μ_{0i}, are obtained from the LR-TDDFT calculations, as previously mentioned. In calculations for the isolated yPy and PyP molecules using the B3LYP functional with the 6-31G basis and the Q_x state as the intermediate state, the two transition dipole moments are 5.1 and 2.3 D in yPy (corresponding to OPA and TPA states at 2.22 and 3.80 eV, respectively), while they are 11.3 and 12.2 D for PyP (for OPA and TPA states at 1.93 and 2.44 eV). When the product of the squares of these transition dipole moments is evaluated, we observe that this factor predicts a TPA cross-section enhancement factor of about 140 in comparing the monomer to the dimer. The actual three-state approximations in these two cases are 66 GM for yPy (compared to 82 GM for this state in Table 5) and 1565 GM for PyP (compared 1870 GM in Table 7). Thus, TDDFT with the B3LYP functional can qualitatively predict, using the three-state model, the enhancement of the TPA that has been observed experimentally; however, once again, the resonance enhancement factor is highly sensitive to the exact state energies, and none of the functionals tested has consistently yielded the accuracy needed for these state energies.

IV. Conclusions

Theoretical OPA and TPA spectra have been calculated with TDDFT for FBP, yPy, and PyP and compared to experimental results. The B3LYP functional was most effective at predicting the OPA, as the CAMB3LYP functional generally overestimated the excitation energy. The overestimation of excited-state energies may be attributed to the additional stabilization of the occupied orbitals that is a result of the inclusion of more exact exchange. It is possible that in CAMB3LYP the exchange and correlation have not been properly balanced. Thus, an improved and rigorous parametrization, not yet carried out, is needed and is currently in progress.

The large enhancement of the TPA cross-section for the porphyrin dimer as compared to the porphyrin monomer, observed experimentally, was predicted by the calculations. The prediction of quantitatively correct TPA cross-sections seems to be limited by the accuracy with which the most relevant state energies can be predicted. The prediction of TDDFT/B3LYP that the transition energy for the relevant TPA state in yPy is about 0.5 eV larger than observed experimentally led to a 5-fold overprediction of the TPA cross-section for this molecule. For PyP, the CAMB3LYP functional accurately predicts the TPA cross-section due to the accuracy of the calculated transition energy, while the underestimation of this transition energy by 0.5 eV with mCAMB3LYP and by 0.8 eV with B3LYP leads to an underestimation of the TPA cross-section by factors of 2 and 4, respectively.

Finally, although the results show the need for improved x-c functionals, at the same time, these calculations qualitatively agree with experimental results by predicting the large TPA enhancement for the porphyrin dimer. Because of the sensitivity of the TPA cross-section to small changes in state energies, a method which will accurately predict state energies is necessary for quantitative prediction of TPA spectra.

Acknowledgment. Computational resources for this research have been provided by the Air Force Research Laboratory High Performance Computing Major Shared Resource Center. We would like thank the Agren group for providing a modified version of the Dalton program which included the CAM-B3LYP (x-c) functional and the PCM solvation model.

Supporting Information Available: The Cartesian coordinates of all of the optimized geometries used in this study are given. OPA and TPA spectra calculated for the yPy and PyP systems with additional basis sets are also listed. This information is available free of charge via the Internet at http://pubs.acs.org.

References

(1) Karotki, A.; Kruk, M.; Drobizhev, M.; Rebane, A.; Nickel, E.; Spangler, C. W. *IEEE J. Selected Top. Quantum Electron.* **2001**, *7*, 971.

(2) Spangler, C. W.; Starkey, J. R.; Meng, F.; Gong, A.; Drobizhev, M.; Rebane, A.; Moss, B. *Optical Methods for Tumor Treatment and Detection: Mechanisms and Techniques in Photodynamic Therapy XIV*; SPIE: Bellingham, WA, 2005; Vol. 5689, p 141.

(3) Bhawalkar, J. D.; Kumar, N. D.; Zhao, C.-F.; Prasad, P. N. *J. Clin. Lasers Med. Surg.* **1997**, *15*, 201.

(4) Aijun, G.; Fanqing, M.; Starkey, J. R.; Moss, B. L.; Rebane, A.; Drobizhev, M.; Spangler, C. W. *ACS Polymeric Materials: Science and Engineering*; American Chemical Society: Washington, DC, 2006; Vol. 95, p 289.

(5) Photofrin Web site. www.photofrin.com (accessed May 2008).

(6) Mansour, K., Jr.; Perry, K. J.; Choong, I.; Marder, S. R.; Perry, J. W. *Proc. SPIE* **1993**, *1853*, 132.

(7) Perry, J. W.; Mansour, K.; Lee, I.-Y. S.; Wu, X.-L.; Bedworth, P. V.; Chen, C.-T.; Ng, D.; Marder, S. R.; Miles, P.; Wada, T.; Tian, M.; Sasabe, H. *Science* **1996**, *273*, 1533.

(8) Su, W.; Cooper, T. M.; Brant, M. C. *Chem. Mater.* **1998**, *10*, 1212.

(9) Karotki, A.; Drobizhev, M.; Dzenis, Y.; Taylor, P. N.; Anderson, H. L.; Rebane, A. *Phys. Chem. Chem. Phys.* **2004**, *6*, 7.

(10) Drobizhev, M.; Stepanenko, Y.; Dzenis, Y.; Karotki, A.; Rebane, A.; Taylor, P. N.; Anderson, H. L. *J. Am. Chem. Soc.* **2004**, *126*, 15352.

(11) Drobizhev, M.; Stepanenko, Y.; Dzenis, Y.; Karotki, A.; Rebane, A.; Taylor, P. N.; Anderson, H. L. *J. Phys. Chem. B* **2005**, *109*, 7223.

(12) Edwards, L.; Dolphin, D. H.; Gouterman, M.; Adler, A. D. *J. Mol. Spectrosc.* **1971**, *38*, 16.

(13) Even, U.; Jortner, J. *J. Chem. Phys.* **1982**, *77*, 4391.

(14) Serrano-Andres, L.; Merchan, M.; Rubio, M.; Roos, B. O. *Chem. Phys. Lett.* **1998**, *295*, 195.

(15) Cai, Z.-L.; Crossley, M. J.; Reimers, J. R.; Kobayashi, R.; Amos, R. D. *J. Phys. Chem. B* **2006**, *110*, 15624.

(16) Cortina, H.; Senent, M. L.; Smeyers, Y. G. *J. Phys. Chem. A* **2003**, *107*, 8968.

(17) Tokita, Y.; Hasegawa, J.; Nakatsuji, H. *J. Phys. Chem. A* **1998**, *102*, 1843.

(18) Yamamoto, S.; Tatewaki, H.; Kitao, O.; Diercksen, G. H. F. *Theor. Chem. Acc.* **2001**, *106*, 287.

(19) Kitao, O.; Ushiyama, H.; Miura, N. *J. Chem. Phys.* **1999**, *110*, 2936.

(20) Hasegawa, J.-y.; Takata, K.; Miyahara, T.; Neya, S.; Frisch, M. J.; Nakatsuji, H. *J. Phys. Chem. A* **2005**, *109*, 3187.

(21) Gwaltney, S. R.; Bartlett, R. J. *J. Chem. Phys.* **1998**, *108*, 6790.

(22) Aspuru-Guzik, A.; Akramine, O. E.; Grossman, J. C.; Lester, W. A. J. *J. Chem. Phys.* **2004**, *120*, 3049.

(23) Masthay, M. B.; Findsen, L. A.; Pierce, B. M.; Bocian, D. F.; Lindsey, J. S.; Birge, R. R. *J. Chem. Phys.* **1986**, *84*, 3901.

(24) Bauernschmitt, R.; Ahlrichs, R. *Chem. Phys. Lett.* **1996**, *256*, 454.

(25) van Gisbergen, S. J. A.; Rosa, A.; Ricciardi, G.; Baerends, E. J. *J. Chem. Phys.* **1999**, *111*, 2499.

(26) Nguyen, K. A.; Day, P. N.; Pachter, R. *J. Phys. Chem. A* **2000**, *104*, 4748.

(27) Šeda, J.; Burda, J. V.; Brázdová, V.; Kapsa, V. *Int. J. Mol. Sci.* **2004**, *5*, 196.

(28) Fabian, J.; Diaz, L. A.; Seifert, G.; Niehaus, T. *THEOCHEM* **2002**, *594*, 41.

(29) Sundholm, D. *Phys. Chem. Chem. Phys.* **2000**, *2*, 2275.

(30) Rumi, M.; Ehrlich, J. E.; Heikal, A. A.; Perry, J. W.; Barlow, S.; Hu, Z.; McCord-Maughon, D.; Parker, T. C.; Rockel, H.; Thayumanavan, S.; Marder, S. R.; Beljonne, D.; Bredas, J.-L. *J. Am. Chem. Soc.* **2000**, *122*, 9500.

(31) Sutherland, R. L. *Handbook of Nonlinear Optics*; Marcel Dekker, Inc.: New York, 1996.

(32) Day, P. N.; Nguyen, K. A.; Pachter, R. *J. Phys. Chem. B* **2005**, *109*, 1803.

(33) Day, P. N.; Nguyen, K. A.; Pachter, R. *J. Chem. Phys.* **2006**, *125*, 094103.

(34) Orr, B. J.; Ward, J. F. *Mol. Phys.* **1971**, *20*, 513.

(35) Birge, R. R.; Pierce, B. M. *J. Chem. Phys.* **1979**, *70*, 165.

(36) Birge, R. R.; Bennett, J. A.; Hubbard, L. M.; Fang, H. L.; Pierce, B. M.; Kliger, D. S.; Leroi, G. E. *J. Am. Chem. Soc.* **1982**, *104*, 2519.

(37) Peticolas, W. L. *Annu. Rev. Phys. Chem.* **1967**, *18*, 233.

(38) McClain, W. M. *Acc. Chem. Res.* **1974**, *7*, 129.

(39) Monson, P. R.; McClain, W. M. *J. Chem. Phys.* **1970**, *53*, 29.

(40) Gold, A. *Proceedings of the International School of Physics*; Academic: New York, 1969.

(41) McClain, W. M. *J. Chem. Phys.* **1971**, *55*, 2789.

(42) Olsen, J.; Jorgensen, P. *J. Chem. Phys.* **1985**, *82*, 3235.

(43) Furche, F. *J. Chem. Phys.* **2001**, *114*, 5982.

(44) Salek, P.; Vahtras, O.; Guo, J.; Luo, Y.; Helgaker, T.; Agren, H. *Chem. Phys. Lett.* **2003**, *374*, 446.

(45) Birge, R. R.; Zhang, C.-F. *J. Chem. Phys.* **1990**, *92*, 7178.

(46) Dick, B.; Hohlneicher, G. *J. Chem. Phys.* **1982**, *76*, 5755.

(47) Frisch, M. J.; Trucks, G. W.; Schlegel, H. B.; Scuseria, G. E.; Robb, M. A.; Cheeseman, J. R.; Montgomery, J. A., Jr.; Vreven, T.; Kudin, K. N.; Burant, J. C.; Millam, J. M.; Iyengar, S. S.; Tomasi, J.; Barone, V.; Mennucci, B.; Cossi, M.; Scalmani, G.; Rega, N.; Petersson, G. A.; Nakatsuji, H.; Hada, M.; Ehara, M.; Toyota, K.; Fukuda, R.; Hasegawa, J.; Ishida, M.; Nakajima, T.; Honda, Y.; Kitao, O.; Nakai, H.; Klene, M.; Li, X.; Knox, J. E.; Hratchian, H. P.; Cross, J. B.; Adamo, C.; Jaramillo, J.; Gomperts, R.; Stratmann, R. E.; Yazyev, O.; Austin, A. J.; Cammi, R.; Pomelli, C.; Ochterski, J. W.; Ayala, P. Y.; Morokuma, K.; Voth, G. A.; Salvador, P.; Dannenberg, J. J.; Zakrzewski, V. G.; Dapprich, S.; Daniels, A. D.; Strain, M. C.; Farkas, O.; Malick, D. K.; Rabuck, A. D.; Raghavachari, K.; Foresman, J. B.; Ortiz, J. V.; Cui, Q.; Baboul, A. G.; Clifford, S.; Cioslowski, J.; Stefanov, B. B.; Liu, G.; Liashenko, A.; Piskorz, P.; Komaromi, I.; Martin, R. L.; Fox, D. J.; Keith, T.; Al-Laham, M. A.; Peng, C. Y. Nanayakkara, A.; Challacombe, M.; Gill, P. M. W.; Johnson, B.; Chen, W.; Wong, M. W.; Gonzalez, C.; Pople, J. A. *Gaussian 03*, A.11.4 ed.; Gaussian, Inc.: Pittsburgh, PA, 2003.

(48) Dalton, a molecular electronic structure program, release 2.0. http://www.kjemi.uio.no/software/dalton/dalton.html (accessed May 2008).

(49) Kruk, M.; Karotki, A.; Drobizhev, M.; Kuzmitsky, V.; Gael, V.; Rebane, A. *J. Lumin.* **2003**, *105*, 45.

(50) Becke, A. D. *Phys. Rev. A* **1988**, *38*, 3098.

(51) Lee, C.; Yang, W.; Parr, R. G. *Phys. Rev. B* **1988**, *37*, 785.

(52) Becke, A. D. *J. Chem. Phys.* **1993**, *98*, 5648.

(53) Vosko, S. H.; Wilk, L.; Nusair, M. *Can. J. Phys. Chem.* **1980**, *58*, 1200.

(54) Stephens, P. J.; Devlin, F. J.; Chabalowski, C. F.; Frisch, M. J. *J. Phys. Chem.* **1994**, *98*, 11623.

(55) Yanai, T.; Tew, D. P.; Handy, N. C. *Chem. Phys. Lett.* **2004**, *393*, 51.

(56) Peach, M. J. G.; Cohen, A. J.; Tozer, D. J. *Phys. Chem. Chem. Phys.* **2006**, *8*, 4543.

(57) Peach, M. J. G.; Helgaker, T.; Salek, P.; Keal, T. W.; Lutnæs, O. B.; Tozer, D. J.; Handy, N. C. *Phys. Chem. Chem. Phys.* **2006**, *8*, 558.

(58) Rudberg, E.; Sałleka, P.; Helgaker, T.; Ågren, H. *J. Chem. Phys.* **2005**, *123*, 184108.

(59) Nguyen, K. A.; Day, P. N.; Pachter, R. *J. Chem. Phys.* **2007**, *126*, 094303.

(60) Tawada, Y.; Tsuneda, T.; Yanagisawa, S.; Yanai, T.; Hirao, K. *J. Chem. Phys.* **2004**, *120*, 8425.

(61) Vydrov, O. A.; Scuseria, G. E. *J. Chem. Phys.* **2006**, *125*, 234109.

(62) Jacquemin, D.; Perpète, E. A.; Vydrov, O. A.; Scuseria, G. E.; Adamo, C. *J. Chem. Phys.* **2007**, *127*, 094102.

(63) Mikkelsen, K. V.; Dalgaard, E.; Swanstrøm, P. *J. Phys. Chem.* **1987**, *91*, 3081.

(64) Mikkelsen, K. V.; Agren, H.; Jensen, H. J. A.; Helgaker, T. *J. Chem. Phys.* **1988**, *89*, 3086.

(65) Tomasi, J.; Mennucci, B.; Cammi, R. *Chem. Rev.* **2005**, *105*, 2999.

(66) Frediani, L.; Rinkevicius, Z.; Agren, H. *J. Chem. Phys.* **2005**, *122*, 244104.

(67) Zhu, Y.; Zhou, S.; Kan, Y.; Su, Z. *Int. J. Quantum Chem.* **2007**, *107*, 1614.

(68) Agren, H. Personal communication.

(69) Rubtsov, I. V.; Susumu, K.; Rubtsov, G. I.; Therien, M. J. *J. Am. Chem. Soc.* **2003**, *125*, 2687.

(70) Zhu, L.; Yi, Y.; Shuai, Z.; Schmidt, K.; Zojer, E. *J. Phys. Chem. A* **2007**, *111*, 8509.

(71) Gouterman, M. *J. Mol. Spectrosc.* **1961**, *6*, 138.

CT800080W